10th International Symposium on the Science and Processing of Cast Iron – SPCI10

Determination of the crack propagation direction of fractured ductile cast iron based on the characteristic features of the surface

D.Fernandino[1*], R.Boeri[1]

[1]Metallurgy Division, National University of Mar del Plata
INTEMA- CONICET, Mar del Plata, Argentina

In this article, the characteristic fractographic features of ductile cast irons with different metallic matrices were analysed. Several heat treatment cycles were carried out on samples from the same cast iron melt in order to obtain ferritic ductile iron, pearlitic ductile iron and austempered ductile iron. The specimens were broken under impact and bending tests and the fracture surfaces were analysed by means SEM observation. Two methodologies to evaluate the main crack propagation based on some characteristic features of the fracture surface were proposed.
The investigation involves a systematic study of the fracture surfaces of ductile iron of different matrices. The authors propose methodologies suitable for identifying the main crack propagation direction of fracture processes of unknown origin applicable to brittle and ductile fracture cases.

Keywords: ductile iron, fracture surface, roughness, bending, crack propagation

Introduction

Ductile irons (DI) can cover a wide range of mechanical properties. Different matrix microstructures can be generated after heat treatments, such as ferritic, pearlitic, martensitic and ausferritc (austempered), among others[1]. Thanks to their good mechanical performance and relatively lower cost when compared to steels, ductile cast irons are increasingly applied in the construction of highly stressed parts of machines and vehicles. The relationship between microstructural features of the material and the working conditions on the DI fracture processes are analysed in the literature by different authors [2-8]. The fractographic characteristics identified for DI differ from those usual in steels and other metallic alloys [9, 10]. The presence of spheroidal graphite and the occurrence of microsegregation can have a strong influence on the morphology of the fracture surface [11, 12]. However, the fractographic analyses reported in most works are secondary to studies of mechanical properties. Few authors have carried out a systematic analysis focused on the interpretation of the DI fracture surfaces under different load conditions [13-15]. Therefore, there is limited information available to evaluate, for example, the crack propagation direction from the observation of some characteristic features of the fracture surface of a component failed in service. This lack of information can be considered to be an obstacle for the application of these alloys because, for example, it is very difficult to extract information from a fractographic analysis and, therefore, to obtain information from one of the more important diagnosis elements.
In consequence, this study is intended to identify the general features of fracture of different types of ductile irons broken under different loading conditions, and to correlate these features with the main crack propagation direction.

Experimental Procedure

The material used in this study was obtained from one-inch 'Y' blocks of DI. The chemical composition was determined by using a Baird DV6 spectrometer. Pearlitic DI was obtained from as-cast condition. 'Y' blocks were ferritised in order to improve the machinability and to standardise the initial microstructure before other heat treatments were carried out. Ferritizing consisted of an austenitizing stage at 920 ºC for 4 hours followed by a slow cooling stage down to room temperature. In addition, a conventional austempering heat treatment cycle consisting of an austenitizing stage at 920°C for 1 hour followed by an isothermal heat treatment at 360°C for 1 hour was made in order to obtain ADI. Metallographic samples were prepared by means standard polishing and etching methods using nital (2 %). The microconstituents as well as the as-cast characterisation were quantified by using an optical microscope OLYMPUS PMG3 and the Image Pro Plus software. V-notched Charpy impact specimens of 10x10x55 mm for impact and three point bending test (ASTM E23) were machined from the 'Y' blocks.

Impact and three point bending tests were carried out. Impact testing was carried out by using a pendulum AMSLER 130/688, with a maximum energy of 300J. Three-point bending tests under quasistatic loading were performed by using a universal testing machine Morh&Federhaff with a crosshead displacement rate of 8.4×10^{-3} mm/sec. The fracture surfaces of the broken specimen were observed by means of a scanning electron microscopy (SEM). Table 1 exemplifies the labelling used to identify the samples for each testing conditions.

* Corresponding author, email: dfernandino@fi.mdp.edu.ar

Table 1. Labelling used for each test condition.

Sample Label	Test type	Test temperature
PI-20	Impact	-20°C
FI-20		
ADI_{360}I-20		
PI20		20°C
FI20		
ADI_{360}I20		
PI60		60°C
FI60		
ADI_{360}I60		
Pflx	Bending	20°C
Fflx		
ADI_{360}flx.		

Results and Discussion

Chemical composition and microstructures

The chemical composition of the DI used is listed in table 2. The as-cast microstructure characterization according with the ASTM A 247 standard and the Brinell hardness are listed in tables 3 and 4 respectively. The nodularity was considered suitable for this study. The microstructures of the different types of samples used are shown in Fig. 1.

Table 2. Chemical Composition of DI used (Wt %)

C	Si	Mn	S	P	Mg	Cu	Ni	Cr
3.32	2.36	0.31	0.012	0.016	0.033	0.62	0.025	0.058

Table 3. Metallographic characterisation of as-cast samples

Nodule count [nod/mm^2]	Nodularity	Nodule size
100	>95%	6

Table 4. *Brinell hardness value*

F	P	ADI_{360}
149	272	350

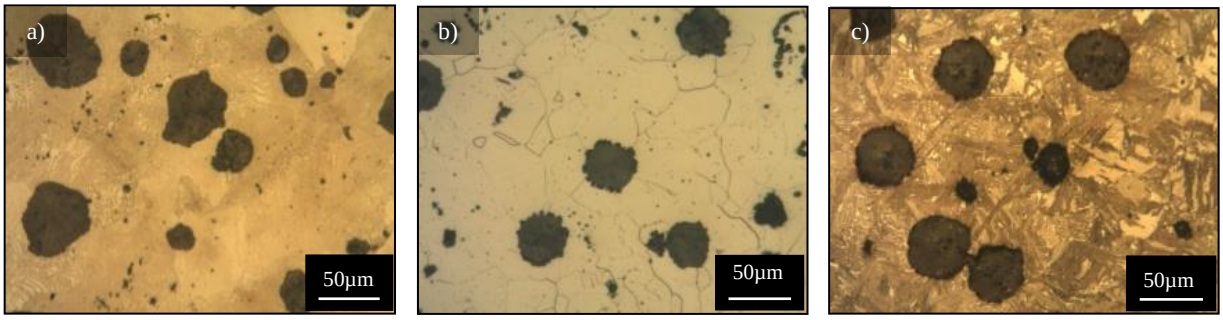

Fig. 1. Microstructures of the different types of DI investigated. (a) Pearlitic (As Cast); (b) Ferritic; (c) Ausferritic.

Analysis of fracture surfaces by SEM

Figures 2 to 5 show several fracture surfaces. A general feature of all fracture surfaces analysed is the presence of graphite nodules and empty cavities left by graphite nodules that were detached from the matrix during the fracture process.

Fracture surfaces from impact testing at different temperatures

Fig. 2 shows the fracture surfaces of ferritic DI impact tested at different temperatures. At low temperatures (-20 ºC, Fig. 2a) the surface shows cleavage facets with river patterns. The graphite nodule cavities show very little strain. Both observations support a predominantly brittle failure mode. At room temperature (Fig. 2b) a significant fraction of the surface shows ductile dimples, while the remaining surface shows cleavage facets. Furthermore, the nodule cavities show extensive deformation. As the test temperature rises to 60 ºC, Fig. 2c, cleavage facets are no longer present, but the fracture surface is dominated by dimples formed after microvoid coalescence.

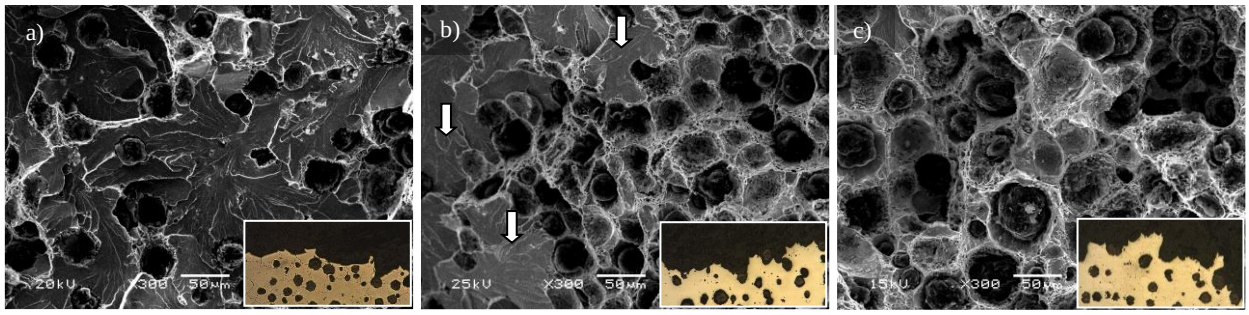

Fig. 2. Fracture surface of FDI broken at different impact test temperature. (a) FI-20; (b) FI20; (c) FI60

Fig. 3 shows the fracture surfaces of pearlitic DI generated by impact testing at different temperatures. A brittle fracture surface conformed by cleavage facets that show river patterns and cracks that break into the surface is observed at -20°C as is shown in Fig. 3a. As the test temperature increases, the predominant fracture mode remains unchanged and only a slight decrease in the number of cracks that break into the surface was found. Even for the samples tested at 60°C, the nodular contours showed little or no plastic strain (Fig. 3c). Only some very small ductile fracture regions were found both at high and low temperatures. Therefore, cleavage facets dominate the fracture surface of pearlitic DI broken under impact, with a minor presence of ductile fracture surfaces.

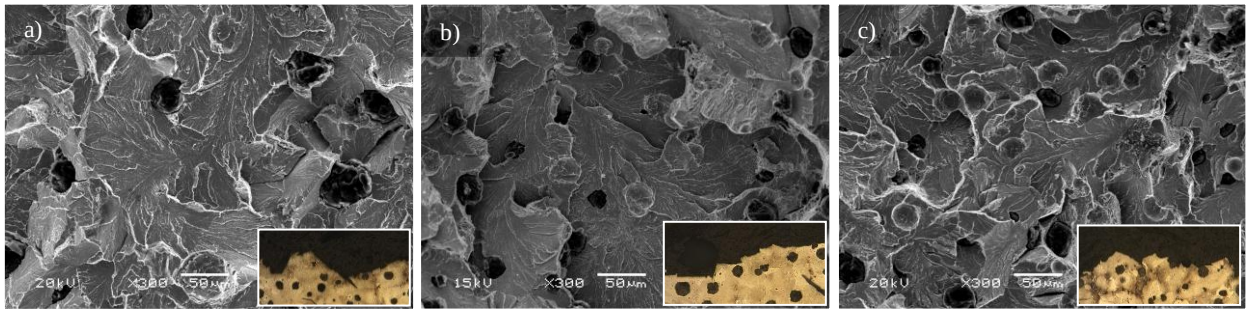

Fig. 3. Fracture surface of pearlitic DI broken by impact at different temperatures. (a) PI-20; (b) PI20; (c) PI60

Fig. 4 shows the fracture surfaces of austempered DI. At low temperature (-20°C, Fig. 4a), the predominant fracture mode is cleavage. Nevertheless, the cleavage facets are smaller than those found in pearlitic and ferritic DI. In addition, the contours of nodular cavities are strained and some disperse areas of ductile fracture can be found. The fracture mechanism combining cleavage facets and small ductile portions is called quasi-cleavage. As the test temperature increased, the nodular contours show greater plastic deformation and the contours of the inclusions, mostly concentrated at the last to freeze portions of the matrix, also show marked deformation. As the temperature further increases, the classical ductile fracture mechanisms begins to be predominant (nucleation, growth and coalescence of voids with the contours of nodular cavities deformed), and the main fracture mechanism changes from quasi-cleavage to ductile (with small areas of quasi-cleavage facets).

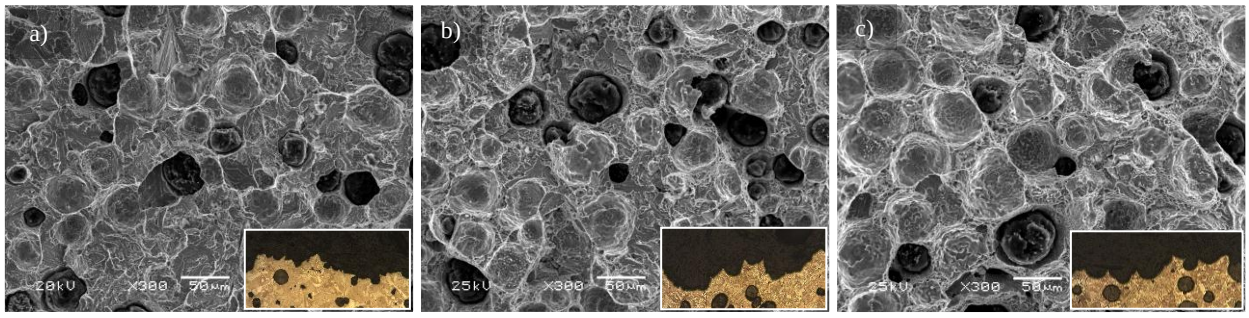

Fig. 4. Fracture surface of ADI broken at different impact test temperature. (a) ADII-20; (b) ADII20; (c) ADII60

Fracture surfaces from bending tests

Fig. 5a shows the fracture surface of ferritic DI. A fully ductile fracture micromechanism dominates the surface, as dimples and highly deformed graphite nodule cavities are found. No cleavage facets are seen. Noticeable differences in the predominant fracture mode are observed as the fracture surfaces broken at room temperature (20ºC) by impact and quasi/static bending loading are compared. After the three-point bending test, the fracture surface shows a very rough topography and a much higher apparent nodular density (i.e. the number of nodules per area) when compared to the fracture surface resulting from the impact testing, where some disperse cleavage facets can be found, as shown in Fig. 2b. This apparently higher nodular density is caused by the greater enlargement of the nodular cavities due to the plastic deformation that takes place when the loading is slow. When pearlitic DI fracture surfaces are analysed, Fig. 5b, brittle cleavage facets dominate the fracture surface and only little portions showing microplasticity features were evidenced along some cleavage steps and other disperse areas of the fracture surface. Consequently, as was reported for the samples broken under impact testing at room temperature, brittle fracture was the predominant failure mode. When fracture surfaces of austempered DI are analysed, several cleavage zones are evidenced (marked by arrows) as shown in Fig. 5c, mixed with ductile fracture portions, resembling the results of impact testing at 60ºC (Fig. 4c).

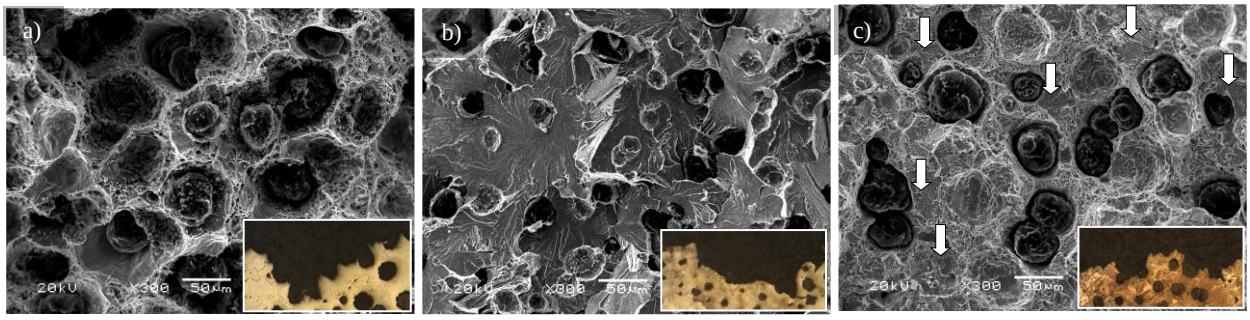

Fig. 5. Fracture surface of samples broken under slow bending testing. (a) Fflx; (b) Pflx; (c) ADIIflx

Main crack propagation direction and its relation with the topographic features

With the goal of identifying the propagation direction of fracture, the topographic features of the fracture surfaces were analysed carefully, for the different loading conditions investigated.

Brittle failure mode

The literature reports that the river patterns present on the cleavage facets converge into a single crack following the direction of the local crack propagation. Therefore, it should be possible to assess the main crack direction through the observation of the propagation on the cleavage planes or facets. The approach used in this study was to identify and to characterize the local propagation direction by means of the observation of the directions of the river patterns with respect to the main crack propagation direction, which is known. The methodology proposed used a local propagation vector that is defined at the point in which two river patterns join, as shown in Fig. 6. All measured local propagation vectors were characterised by the angle formed with respect to the main crack propagation direction. The large number of values of local angles measured were averaged and the resulting direction compared to the main crack propagation direction. In all situations, the main crack propagation direction was set at 0 º.

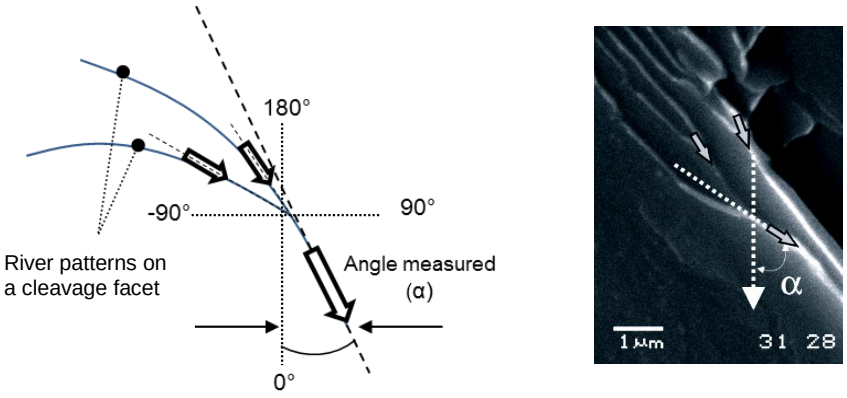

Fig. 6. Method used to define a local propagation vector on the cleavage fracture surfaces resulting of impact and bending test.

The results of the statistical dataset are listed in Fig. 7. The mean value (X) of the dataset was 9±2 and the mode value (Mo) of the distribution was 0º. These results not only show that the average of local propagation vectors reveals the predominant propagation direction with good accuracy, but also, a higher relative frequency was observed for the directions with little deviation from the main crack propagation. The local directions were grouped into 20 intervals ranging from -180º to 180º in concordance with the reference system used in the present methodology. A number of 1515 local crack propagation direction was analysed in five different fracture surface area.

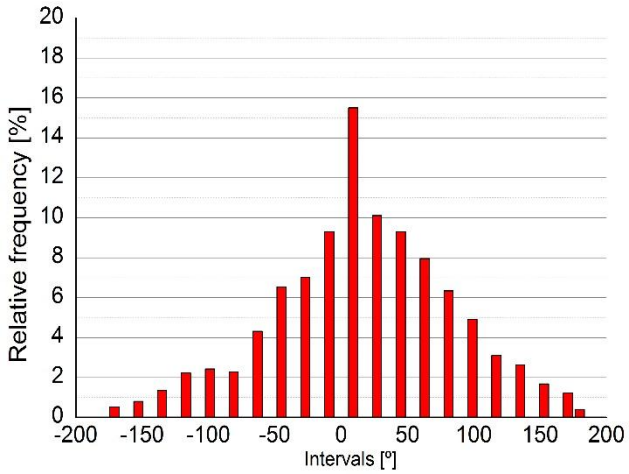

Fig. 7. Histogram obtained from the quantitative analysis on SEM fractographies of FI-20 sample.

Ductile failure mode

A different method was developed to determine the propagation direction when the ductile fracture is the predominant failure mode. The method is based on the measurement of the plastic deformation of the metallic matrix surrounding the graphite nodules. For each nodule present at the fracture surface an ellipse is manually defined with the best possible fit to the deformed nodular contour. Then, two different measurements were carried out. First, the length of the nodular contour in parallel (Y) and perpendicular (X) axes to the main crack propagation direction were measured, as shown in Fig. 8. In addition, the angle formed between the major axis of the ellipse and the main crack propagation direction was measured. The methodology demands time and care. The results of the measurements of the ratio Y/X and the angle (α) on several fields of the samples investigated are listed in table 4. The results are grouped depending on the value of the Y/X ratio. The larger proportion of the nodular cavities show values of Y / X greater than 1, i.e., the nodular cavities tended to strain according to the main crack propagation.

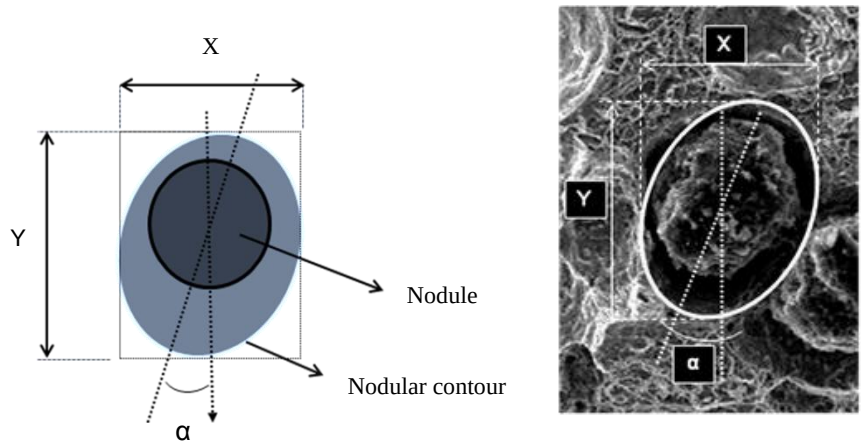

Fig. 8. Method used to measure the parameters that characterise the nodule contour deformation. Ductile fracture.

Table 5. Deformation of the nodular contour on the fracture surface

Sample	Y axe [%]	Equiaxial [%]	X axe [%]	Contours analysed	Angle (β)
FI60	66	23	10	254	2.70 ± 0.18º
Fflx	77	15	8	135	0.80 ± 0.14º
ADI_{360}I-20	72	6	23	74	1.90 ± 0.28°
ADI_{360}I60	68	7	24	111	2.20 ± 0.30°
ADI_{360}Flx	78	11	12	161	9.00 ± 0.20º

For a better interpretation of the dataset, a histogram and a function of cumulative frequency of the X/Y ratio is plotted in Fig.9. The results show that for the ferritic DI sample under impact testing at 60°C, 66% of the nodular cavities analysed had a ratio Y/X> 1, while for the bending case, this value increased to 77%. For ADI, in all test conditions, the ratio Y/X was greater than one for at least the 68% of the dataset. The fraction of the nodular contours showing greater deformation along the Y-axis increase as the impact test temperature increases, and as loading in quasistatic. The mean values of β show a maximum deviation respect to the reference Y- axe of 9.00 ± 0.20° for ADI_{360}I-20 sample. The average of β values obtained in each condition for each DI were plotted in Fig. 10. Taking into account that the reference Y-axis has been set along the main crack propagation direction, it can be concluded that this method allows to identify the main crack propagation direction with good approximation. It must be noted that the result will be independent from the reference axis chosen, as will be the case when a fracture surface of unknown crack propagation direction is examined.

a)

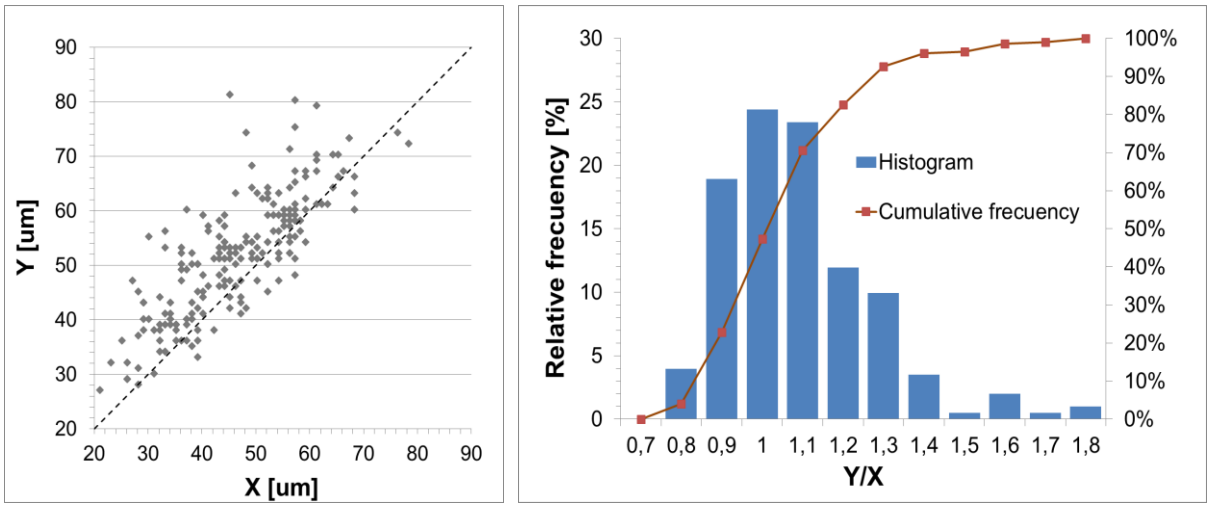

b)

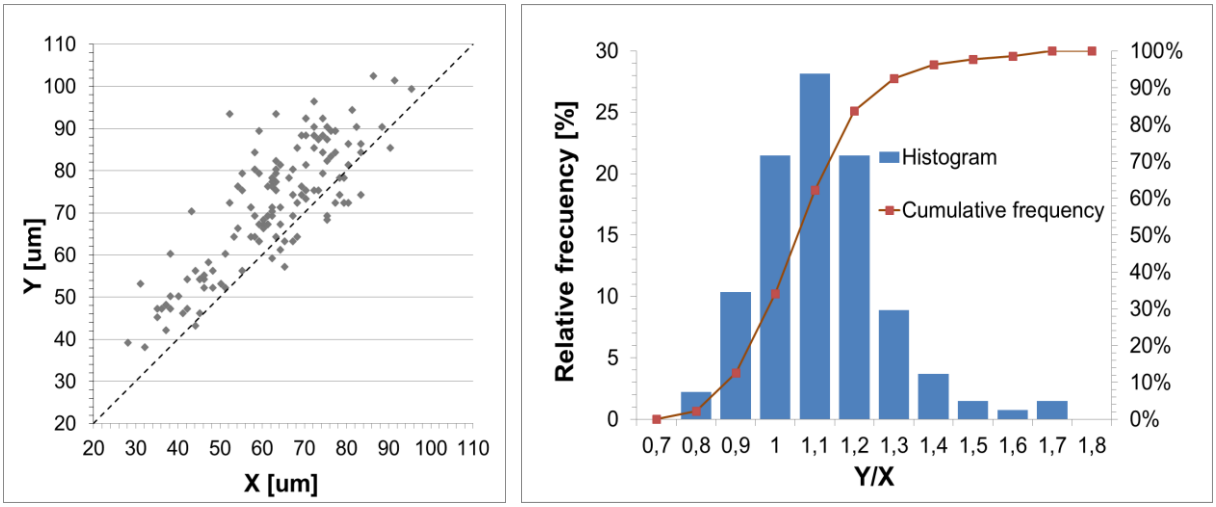

Fig. 9. Statistic plots from the experimental measurements of X/Y ratio on FDI. (a) FI60; (b) Fflx

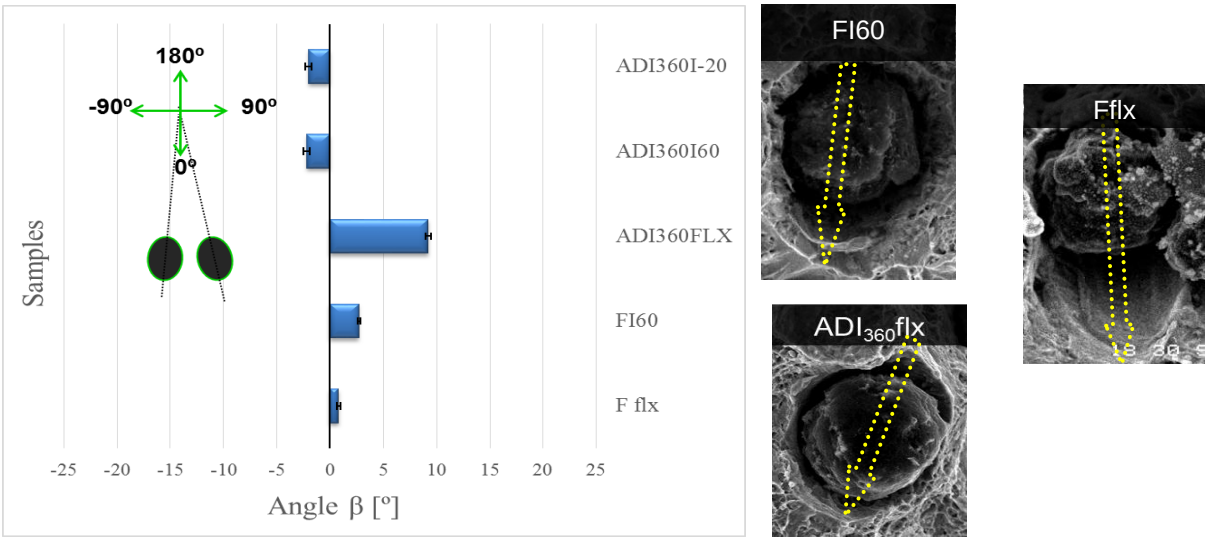

Fig. 10. Plot from the experimental measurements of angle $_{\beta}$

Conclusions

The investigation involves a systematic study of the fracture surfaces of DI with different metallic matrices and broken under different loading conditions.

1. In the case of ferritic ductile iron, the predominant failure mode shows noticeable changes as a function of the loading conditions and testing temperatures. The predominant fracture mechanism changes from brittle (cleavage) to ductile as the impact test temperature increases. When fracture surface from bending test was evaluated, a fully ductile behavior was evidenced.
2. In the case of pearlitic ductile iron the fracture surfaces resulting from both impact at different temperatures and bend loading, showed brittle fracture characteristics, as the surfaces were conformed by cleavage facets that show river patterns and cracks that break into the surface. Only some very small ductile fracture regions were found at both high and low testing temperatures.
3. In austempered ductile iron the predominant fracture mechanism change from quasi-cleavage to ductile (with little areas of cleavage facets) as the impact testing temperature was increased. For bending test, a mix of cleavage facets, nodular contours strain and microvoids coalescence were evidenced. The contours of the inclusions, mostly concentrated at the last to freeze portions of the matrix, also show marked deformation.
4. Complex but reliable methodologies for the determination of the main crack propagation direction were proposed. For brittle fracture, the method is based on a careful analysis of the river patterns along the cleavage planes. For

ductile fracture, the method is based on the measurement of the plastic deformation of the metallic matrix surrounding the graphite nodules.

References

1. Ductile Iron Data for Design Engineers (1990). Cap. II Introductions.
2. Di Cocco, F.Iacoviello, M Cavallini. *Engineering fracture Mechanics*, 2010, 77, 2016-2023.
3. D. Rajnovic, O. Eric, L. Sidjanin. *Journal of Microscopy*, 2008, 232, 605–610.
4. L.Eldoky, R.C.Voigt. Fracture of Ferritic Ductile Cast Iron. Transactions of the American Foundrymen's Society.Vol.94; Minneapolis, Minnesota; USA; 12-15, 1986. 621-630.
5. F.Iacoviello, O.Di Bartolomeo, V.Di Cocco, V.Piacente. *Materials science and Engineering A*, 2008, 478, 181-186.
6. G.L.Greno, J.L.Otegui, R.E.Boeri. *Int. J. of fatigu*e, 1999, 21, 35-43.
7. M.F. Hafiz, A. Hammouda, S. El-Gemae. AFS Transactions 2005 American Foundry Society, Schaumburg, II. USA 2-12.
8. R. Konecna, P. Lejcek, G. Nicoletto and P. Bartuska. Materials Science and Technology, 2006, 22, 1415-1422.
9. T-L.Anderson. (1995) Fracture Mechanics. Fundamentals and Applications. 2nd ed., pp. 265-305.
10. Broek D. Elementary engineering fracture mechanics. (1991) 4th ed. 101 Philip Dr., Norwell, MA 02061 USA: Kluwer Academic Publishers.
11. P.Q.Dai, Z.R.He, C.M.Zheng, Z.Y.Mao. *Materials Science and Engineering A, 2001,* 319-321, 531-534.
12. R.C.Voigt, L.M.Eldoky. Transactions of the American Foundrymen's Society. Minneapolis, Minnesota; USA; 12-15 May 1986, 94, 637-644.
13. A. Ghahremaninezhad, K. Ravi-Chandar. Acta Materialia, 2012, 60, 2359–2368
14. R.A.Martinez. *Engineering Fracture Mechanics* 2010, 77, 2749–2762.
15. V. M. Bermont, R. N. Castillo and J. A. Sikora. ISIJ International, 2002, 42, 1303–1308

Acknowledgement

The authors are grateful to CONICET and the National University of Mar del Plata for their financial support.